2021 43rd Annual International Conference of the
IEEE Engineering in Medicine & Biology Society (EMBC)
Oct 31 - Nov 4, 2021. Virtual Conference

Selective myelinated nerve fiber stimulation via temporal interfering electric fields

Gonglei Wang and Socrates Dokos, *Member, IEEE*
Graduate School of Biomedical Engineering, UNSW Sydney

Abstract— We have investigated selective electrical stimulation of myelinated nerve fibers using a computational model of temporal interfering (TI) fields. The model consists of two groups of electrodes placed on the outer bundle surface, each group stimulated at a different frequency. We manipulated the stimulus waveform, magnitude and frequency of short-duration stimuli (70ms), and investigated fiber-specific stimulus-elicited compound action potentials. Results show that under 100Hz & 200Hz TI stimulation with 0.6mA total current shared by the electrodes, continuous action potentials were generated in deeper nerve fibers, and that the firing region was steerable by changing individual electrode currents. This study provides a promising platform for non-invasive nerve bundle stimulation by TI fields.

Keywords — temporal interfering (TI); computational modelling; selective stimulation; nerve fiber stimulation;

I. Introduction

Use of temporal interfering (TI) fields for nerve stimulation (TI), such as vagus nerve stimulation (VNS), have led to widespread excitement about the possible treatment of various neural conditions, including epilepsy, depression and cluster headaches [1-5]. There is also growing interest in using TI to treat other conditions, including heart failure, rheumatoid arthritis, inflammatory bowel disease, ischemic stroke and traumatic brain injury, many of which are characterized by inflammation [6-8]. Extensive pre-clinical evidence has demonstrated the utility of TI in treating inflammatory conditions, and further supports its widespread application [9,10].

Recently, a non-invasive steerable method has been proposed by Grossman *et al.* [3]. They found that high-frequency electric field temporal interactions of fields of different frequency can be used to selectively activate deeper neurons in a nerve bundle or brain cortex [11-14]. In particular, if two groups of electrodes, each stimulating with different frequency, are placed at multiple sites outside a nerve bundle, the resulting interference will generate an envelope waveform oscillating at half the frequency difference of the two fields. If the maximum envelope amplitude is high enough in the inner nerve bundle, it might be possible to selectively activate deep-lying neurons. One study has indicated that TI stimulation may be an effective method for non-invasive deep brain stimulation in mice [15].

This study explores the possibility of using TI fields to selectively activate myelinated neurons in the inner region of a nerve bundle using computational modelling. We also examined the steerability of the activated region without physically altering electrode positions.

II. Methods

The finite element modelling software used was COMSOL Multiphysics 5.5. The nerve bundle geometry, as shown in Fig.1a, was defined as a cylinder 5 mm length and 1mm radius. A series of axon fibers were defined as embedded edge elements distributed in 5×5 lattice, spaced 0.25 mm apart, and centred along the nerve axis. Four square external cuff electrodes of size 1×1mm were wrapped equi-spaced around the bundle surface. Two were active and the other two were ground electrodes, as shown in Fig. 1a.

All nerve fibers were modeled as myelinated, consisting of nodes (unmyelinated parts) and internodes (myelinated parts). Each internode segment was much longer (1000 μm) than each node segment (1 μm) [16]. The radius of each fiber was fixed at 2.5 μm, with the conceptual structure of the fibers shown in Fig.1b.

A distributed resistance boundary condition was incorporated at the ends of each fiber, as given by Eq.1.

$$J = \frac{V_r - V_m}{\rho L} \qquad (1)$$

J is the inward axial current at the fiber ends
V_r is the resting potential potential, in mV
V_m is the fiber membrane potential at the boundary, in mV
ρ is the fiber axial resistivity, in Ω • m
L is the nominal distance between the boundary and a remote segment at resting membrane potential, in m. This distance should be greater than the length constant of the fiber.

The model also included line current sources for each node, to account for the effect of nodal membrane currents on the applied extracellular electric field due to the stimulating electrodes. Defining Q as the outward nerve membrane current per unit length along the axon, we have:

$$Q = 2\pi r \left(C_m \frac{\partial V_m}{\partial t} + i_{ion} \right) \qquad (2)$$

C_m is the membrane capacitance, in F/m^2.

i_{ion} is the ionic current density through the nodal membrane, in A/m^2.

r is the fiber radius, in m.

Ionic currents in the fiber nodes were modelled according to the Hodgkin-Huxley equations [17]:

$$i_{ion} = \bar{g}_{Na} m^3 h (V_m - V_{Na}) + \bar{g}_K n^4 (V_m - V_K) + \bar{g}_L (V_m - V_L)$$

where m, n, h are gating variables, and remaining parameters are given in Table 1. All model parameters are given in Tables 1-3.

To visualize the number of action potential spikes generated in each fiber, we defined an ordinary differential equation (ODE) in variable w according to Eq.3. When the membrane potential was positive, w transiently increased in value. The higher the value of w, the longer was the time the fiber was activated (i.e. whenever $V_m > 0$), and the greater the number of spikes generated.

$$\frac{dw}{dt} = \begin{cases} 1 & \text{if } V_m > 0 \\ 0 & \text{Otherwise} \end{cases} \quad (3)$$

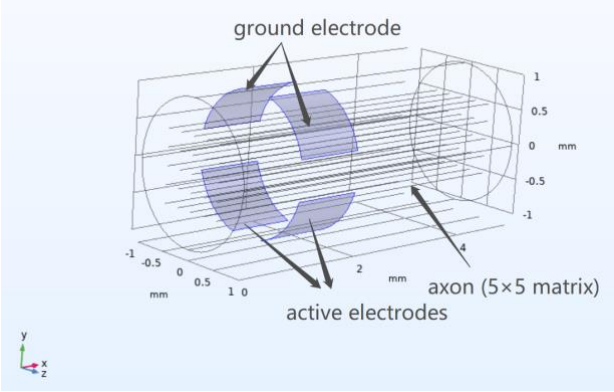

(a)

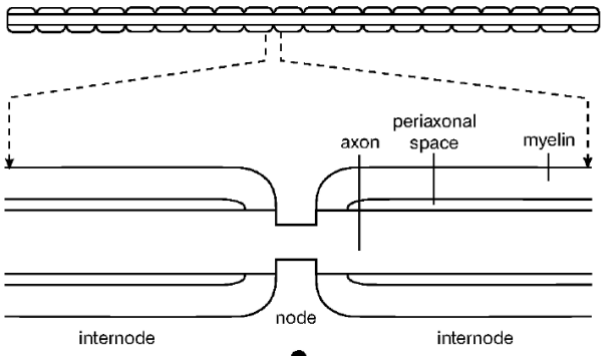

(b)

Figure 1. (a) 3D schematic representation of nerve bundle model containing 5×5 axon fiber lattice and 2 groups of cuff electrodes. The x-axis represents the direction of the nerve fibers. The y-z plane represents the cross section of the nerve bundle. (b) Schematic structure of each myelinated nerve fibre [15].

III. Results and Discussion

We found that TI stimulation could selectively stimulate the inner fibers of the nerve bundle. At 100Hz & 200Hz stimulus frequencies and 0.6 mA total external current, the activated fibers within the bundle are shown as Fig. 2.

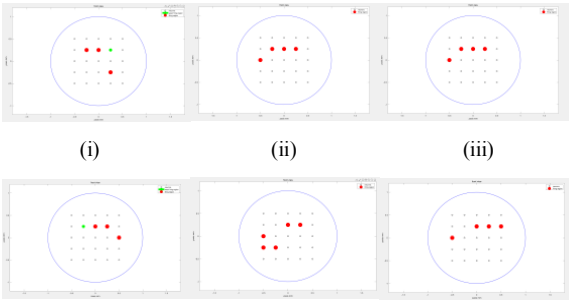

(i) (ii) (iii)

(iv) (v) (vi)

Figure 2. 2D cross-section visualization of activated fibers (w variable) resulting from 100/200 Hz TI stimulation. The upper left and right corner are the ground electrodes. The lower left corner is the higher frequency current source and the lower right corner is the lower frequency current source. Red dots indicate the fibers that produce a train of action potentials with 20 ms interval, green dots show fibers that produce lower frequency spikes, whilst black dots indicate fibers that don't elicit an action potential. (i) 100Hz 0.2mA; 200Hz 0.4mA. (ii) 100Hz 0.25mA; 200Hz 0.35mA. (iii) 100Hz 0.3mA; 200Hz 0.3mA. (iv) 100Hz 0.35mA; 200Hz 0.25mA. (v) 100Hz 0.4mA; 200Hz 0.2mA. (vi) 100Hz 0.45mA; 200Hz 0.15mA.

In each case, the fiber activated region was found to be thin and stripped-shaped, as shown in Fig. 3. By decreasing the fiber-fiber distance of the 5×5 grid, and centering it to a new location in the bundle, we could arbitrarily increase the resolution of the activated region, providing a finer visualization. As shown in Fig. 3, the total area of the thin, activated region was similar under different stimulation conditions, but the activated region shifted slightly toward the electrode with the higher current when changing the electrode current ratio. One potential method to enhance the shift, and hence steerability of the activation region, would be to simultaneously change the position of the cuff electrodes and the ratio of current, but this was not explored further in the current study.

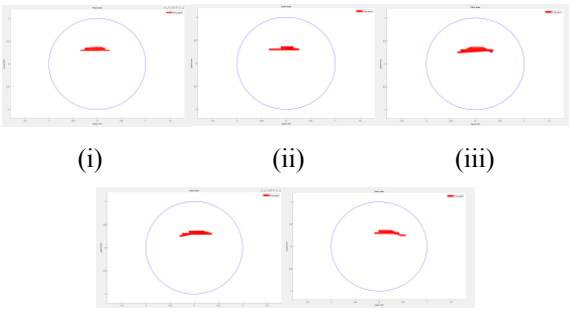

(i) (ii) (iii)

(iv) (v)

Figure 3. 2D visualization of activated fibers at finer resolution of 0.05 mm fiber spacing. The red dots indicate activated fibers, with various panels showing a range of stimulus conditions. (i) 100Hz 0.2mA; 200Hz 0.4mA. (ii) 100Hz 0.25mA; 200Hz 0.35mA. (iii) 100Hz 0.3mA; 200Hz 0.3mA. (iv) 100Hz 0.35mA; 200Hz 0.25mA. (v) 100Hz 0.4mA; 200Hz 0.2mA.

We also observed in our simulations that the myelinated neural structure may promote deep region firing for low frequency TI stimulation. Fig.4 shows results from the case when the 5×5

fibers were modelled as unmyelinated neurons. Under 100Hz 0.3mA/ 200Hz 0.3mA stimulation, the outer neural fibers closest to the cuff electrodes were activated as opposed to the inner ones. Comparing this with the earlier results in Figs. 2 and 3, we see that the myelinated structure itself may promote selective activation of the inner nerve fibers under TI stimulation, although the mechanism underlying this is still unclear.

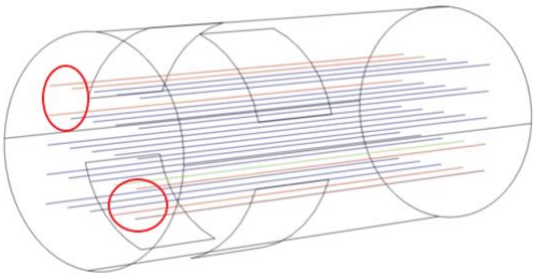

Figure 4. TI stimulation in the case of unmyelinated fibers. Activated fibers are shown in red, highlighted by the red circles around groups of activated fibers. Stimulus conditions were 100 Hz/200Hz with 0.3 mA in each electrode.

Different frequency TI combinations were also implemented in the model, as shown in Table 4. Results indicated that frequency had a significant impact on TI stimulation. As shown in Fig. 5, lower or higher frequencies than the 100-200 Hz range used earlier (see Fig. 5i, ii, iii) only activated the outer fibers. Moreover, a much higher frequency (Fig. 5iv) suppressed neuron firing, requiring a larger external current to stimulate the fibers. Thus, we observed a frequency window in which inner bundle fibers could be selectively activated.

The study did not explore the case of a mixed-fiber nerve bundle model, or using more than two groups of electrodes. Furthermore, nerve bundles typically exhibit a more complex structure, such as different fiber radii, variations in myelin distribution, and heterogeneous fiber densities [23-26]. In future, we hope to carry out simulations using mixed fiber types and more realistic fiber nerve bundle distributions.

IV. Conclusion

In our study, we used different strategies for TI nerve fiber stimulation. Our results showed that TI stimulation can be used for selective myelinated axon fiber stimulation in a nerve bundle. It also indicates the possibility of steerable nerve stimulation motor patterns by changing the cuff electrode current ratio. Furthermore, inner myelinated fibers could be selectively activated by TI stimulation as compared to unmyelinated fibers. We found that for our Hodgkin-Huxley neuron, 100Hz & 200Hz TI fields were the optimal frequencies for selective inner fiber activation. Although there are open questions which still need to be addressed, including the mechanisms underlying the efficacy of TI stimulation in the myelinated fiber case, our results provide in principle support for selective, targeted, non-invasive nerve stimulation. Future work will be focused on mathematical optimization of the TI stimulation, to investigate the internal fiber activation region in the nerve bundle, particularly in the presence of multiple nerve fiber types.

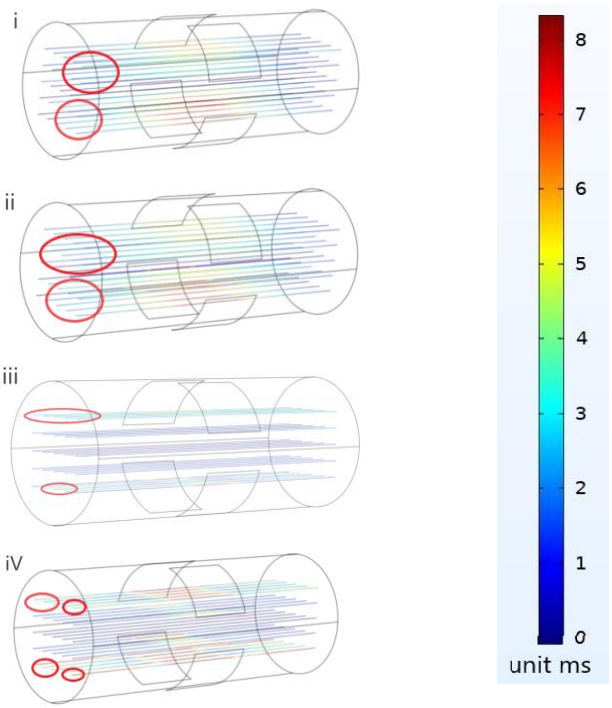

Figure 5. TI stimulation under various frequencies. The color bar shows the total time of positive membrane potential (i.e. $V_m > 0$) in ms, an indicator of the number of spikes generated in each fiber. The red circles in each panel demarcate the activated fiber regions. (i) 50Hz 0.3mA; 100Hz 0.3mA. Outer fibers are activated closest to the electrodes (ii) 50Hz 0.3mA; 150Hz 0.3mA. Again, outer fibers are activated. (iii) 300Hz 0.3mA; 400Hz 0.3mA. Activated fibers are between the two active electrodes and the two ground electrodes in the outer bundle region. (iv) 1000Hz 1mA; 1100Hz, 1mA. Fibers closest to the active and ground electrodes can be activated, but a larger current (1 mA in each active electrode) is required.

Table 1. Nodal Parameters.

Parameter	Value	Unit	Reference
Nodal length	1	μm	[19]
Internodal distance	1000	μm	[29]
Nodal radius (r)	2.5	μm	[18]
Nodal capacitance (C_m)	1	μF/cm^2	[18]
$\bar{g}_{Na}$	120000	μS/cm^2	[21]
$\bar{g}_K$	36000	μS/cm^2	[21]
$\bar{g}_L$	300	μS/cm^2	[21]
V_{Na}	55	mV	[21]
V_K	-72	mV	[21]
V_L	-49.38	mV	[21]
Resting potential	-60	mV	[18]
Nodal resistivity	60	Ω·cm	[18]

Table 2. Internodal parameters.

Parameter	Value	Unit	Reference
Myelin length	1000	um	[16]
Myelin capacitance(c_m)	0	μF/cm^2	[22]
Myelin conductance	0	S/cm^2	[22]
Boundary length (L)	1	cm	

Table 3 Bulk nerve bundle parameters

Parameter	Value	Unit	Reference
Inner space conductance	1	S/cm^2	[18]
Shell conductance	0	S/cm^2	[18]
Nerve bundle radius	1	mm	[18]

Table. 4. Various frequency stimulation conditions simulated.

	Frequency 1		Frequency 2	
	Frequency (Hz)	Current (mA)	Frequency (Hz)	Current (mA)
i	50	0.3	100	0.3
ii	50	0.3	150	0.3
iii	300	0.3	400	0.3
iv	1000	1	1100	1

REFERENCES

[1] Yamamoto, Takamichi, 'Vagus Nerve Stimulation Therapy: Indications, Programing, and Outcomes' (2015) 55(5) Neurologia medico-chirurgica 407

[2] Kumar, A., Bunker, M. T., Aaronson, S. T., Conway, C. R., Rothschild, A. J., Mordenti, G., et al. (2019). Durability of symptomatic responses obtained with adjunctive vagus nerve stimulation in treatment-resistant depression. Neuropsychiatr. Dis. Treat. 15, 457–468. doi: 10.2147/NDT.S196665

[3] Grossman N, Bono D, Dedic N, Kodandaramaiah SB, Rudenko A, Suk HJ, Cassara AM, Neufeld E, Kuster N, Tsai LH, Pascual-Leone A, Boyden ES. Noninvasive Deep Brain Stimulation via Temporally Interfering Electric Fields. Cell. (2017) Jun 1;169(6):1029-1041.e16. doi: 10.1016/j.cell.2017.05.024

[4] Conway, C. R., Gott, B. M., and Azhar, N. H. (2016). "Vagus nerve stimulation for treatment-refractory depression," in Neuromodulation in Psychiatry, eds C. Hamani, P. Holtzheimer, A. M. Lozano, and H. Mayberg, (Hoboken: John Wiley & Sons), 335–352. doi: 10.1002/9781118801086.ch18

[5] Ruffoli, R., Giorgi, F. S., Pizzanelli, C., Murri, L., Paparelli, A., and Fornai, F. (2011). The chemical neuroanatomy of vagus nerve stimulation. J. Chem. Neuroanat. 42, 288–296. doi: 10.1016/j.jchemneu.2010.12.002

[6] Johnson, Rhaya L and Wilson, Christopher G, 'A Review of Vagus Nerve Stimulation as a Therapeutic Intervention' (2018) 11 Journal of inflammation research 203

[7] Hoffmann, Thomas J et al, 'Inhibition of Histamine-Induced Bronchoconstriction in Guinea Pig and Swine by Pulsed Electrical Vagus Nerve Stimulation' (2009) 12(4) Neuromodulation (Malden, Mass.) 261

[8] Ryvlin, Philippe et al, 'The Long-Term Effect of Vagus Nerve Stimulation on Quality of Life in Patients with Pharmacoresistant Focal Epilepsy: The PuLsE (Open Rospective Randomized Ong-Term Ffectiveness) Trial' (2014) 55(6) Epilepsia (Copenhagen) 893

[9] Guiraud, D., Andreu, D., Bonnet, S., Carrault, G., Couderc, P., Hagege, A., et al. (2016). Vagus nerve stimulation: state of the art of stimulation and recording strategies to address autonomic function neuromodulation. J. Neural. Eng. 13:041002. doi: 10.1088/1741-2560/13/4/041002

[10] Koopman, F. A., Chavan, S. S., Miljko, S., Grazio, S., Sokolovic, S., Schuurman, P. R., et al. (2016). Vagus nerve stimulation inhibits cytokine production and attenuates disease severity in rheumatoid arthritis. Proc. Natl. Acad. Sci. U.S.A. 113, 8284–8289. doi: 10.1073/pnas.1605635113

[11] Hutcheon, Bruce and Yarom, Yosef, 'Resonance, Oscillation and the Intrinsic Frequency Preferences of Neurons' (2000) 23(5) Trends in neurosciences (Regular ed.) 216

[12] Miranda, Pedro Cavaleiro et al, 'The Electric Field in the Cortex During Transcranial Current Stimulation' (2013) 70 NeuroImage (Orlando, Fla.) 48

[13] Hutcheon, B., Yarom, Y., 2000. Resonance, oscillation and the intrinsic frequency preferences of neurons. Trends Neurosci. 23 (5), 216–222.

[14] Bikson, M., Inoue, M., Akiyama, H., Deans, J.K., Fox, J.E., Miyakawa, H., Jefferys, J.G.R., 2004. Effects of uniform extracellular dc electric fields on excitability in rat hippocampal slices in vitro. J. Physiol. 557 (1), 175–190.

[15] Kilgore, Kevin L and Bhadra, Niloy, 'Reversible Nerve Conduction Block Using Kilohertz Frequency Alternating Current' (2014) 17(3) Neuromodulation (Malden, Mass.) 242

[16] Richardson, A G, McIntyre, C C and Grill, W M, 'Modelling the Effects of Electric Fields on Nerve Fibres: Influence of the Myelin Sheath' (2000) 38(4) Medical & biological engineering & computing 438

[17] Hodgkin, A. L and Huxley, A. F, 'A Quantitative Description of Membrane Current and Its Application to Conduction and Excitation in Nerve' (1952) 117(4) The Journal of physiology 500

[18] Dokos, Socrates, Modelling Organs, Tissues, Cells and Devices: Using MATLAB and COMSOL Multiphysics (Springer, 2017)

[19] Rydmark, Martin, 'Nodal Axon Diameter Correlates Linearly with Internodal Axon Diameter in Spinal Roots of the Cat' (1981) 24(3) Neuroscience letters 247

[20] Berthold, C H and Rydmark, M, 'Electron Microscopic Serial Section Analysis of Nodes of Ranvier in Lumbosacral Spinal Roots of the Cat: Ultrastructural Organization of Nodal Compartments in Fibres of Different Sizes' (1983) 12(3) Journal of Neurocytology 475

[21] Frankenhaeuser, B and Huxley, A. F, 'The Action Potential in the Myelinated Nerve Fibre of Xenopus Laevis as Computed on the Basis of Voltage Clamp Data' (1964) 171(2) The Journal of physiology 302

[22] McNeal, Donald R, 'Analysis of a Model for Excitation of Myelinated Nerve' (1976) BME-23(4) IEEE transactions on biomedical engineering 329

[23] Tseng, To-Jung et al, 'Determinants of Nerve Conduction Recovery after Nerve Injuries: Compression Duration and Nerve Fiber Types' (2015) 52(1) Muscle & nerve 107

[24] Hendriksen, P H et al, 'Subclinical Diabetic Polyneuropathy: Early Detection of Involvement of Different Nerve Fibre Types' (1993) 56(5) Journal of neurology, neurosurgery and psychiatry 509

[25] Szlavik, Robert B and de Bruin, Hubert, 'The Effect of Stimulus Current Pulse Width on Nerve Fiber Size Recruitment Patterns' (1999) 21(6) Medical engineering & physics 507

[26] Araji, MT and Boubekri, M, 'A Novel Way of Utilising Radiance-Matlab Visualisation for Façade Design Optimisation' (2011) 43(1) Lighting research & technology (London, England: 2001) 103